Effect of silver-nanoparticle aggregation on surface-enhanced Raman scattering from benzoic acid

M. C. Chen, S. D. Tsai, M. R. Chen, S. Y. Ou, W-H. Li, and K. C. Lee
Department of Physics, National Central University, Chung-Li, Taiwan 32054, Republic of China
(Received 11 July 1994)

Silver nanoparticles were fabricated using the gas-evaporation method, and were deposited directly onto various substrates for different measurement purposes. Surface images obtained by transmission electron microscope and atomic force microscope show that the films fabricated consist of Ag nanoparticles rather than a smooth Ag layer or Ag islands. A series of Ag-nanoparticle films fabricated at different evaporation rates but with mass thickness fixed at 100 Å was used to study the surface-enhanced Raman scattering (SERS) from benzoic acid. The major differences among the films fabricated are the degrees of aggregation of Ag nanoparticles, while their mean grain sizes fall in the same length scale. Every film studied exhibits a surface-plasma resonance peak at ~3800 Å with a long tail extending to the visible region, and the extinction of aggregated films is much stronger than that of dispersed films. In emphasizing the electromagnetic effect, the attenuated total-reflection method was employed in obtaining the SERS spectrum, where the excitations of surface plasmons and the enhanced Raman intensities were measured simultaneously. Densely aggregated films give stronger enhancements than dispersed films do, and a factor difference as large as 15 on the enhanced Raman intensities was observed between the most densely and the most loosely aggregated films studied. The enhancements are electromagnetic in nature, and we attribute them to the excitations of surface plasmons.

I. INTRODUCTION

The observation[1] of huge Raman signal from pyridine adsorbed onto electrochemically roughened Ag electrodes has initiated numerous investigations[2,3] on its related topics. Quantitative analyses[4–6] have indicated that the Raman cross section may have been enhanced by a factor as large as 10^6. Any mechanism that is capable of enhancing signals by a factor of 10^6 deserves detailed investigations in every sense. This enhancement phenomenon of electromagnetic radiation by roughened surfaces is nowadays known as surface-enhanced Raman scattering (SERS). That has become a widely used technique in obtaining vibrational spectrum, developing surface analytics, and investigating energy-conversion processes on the surfaces.

The mechanisms for the huge enhancement of Raman signal by roughened surfaces are still puzzling, but fall into two general categories of electromagnetic (EM) and chemical (CHEM) effects. In the long-range EM mechanism,[2,5] the enhancement is originated from the creations of either extended surface plasmon[7,8] (SP) on continuous surfaces or localized particle plasmon[9,10] (PP) on isolated metal-particle surfaces by a strong local electromagnetic field induced by incident light. The short-range CHEM mechanism,[6] on the other hand, asserts that particular chemical bonds between the substrate and the molecules that modify Raman cross section are established by the roughened surfaces.[11] The overall enhancement factor for each of the two mechanisms is still a matter of debate. However, it is in general believed that a factor of 10^4 on the enhancement can be expected from the EM effect, while the CHEM effect may contribute a factor of about 10^2.

At present stage, the EM mechanism is generally of overwhelming importance in most situations studied. Numerous studies[2,3,12] have demonstrated that rough surface consisting of metal islands can support extended SP as well as highly localized PP that appear to be particularly efficient in enhancing electromagnetic radiations.[13–18] Particle plasmons are the plasma oscillations of the conduction electrons on the surface of isolated metal particles. They are localized in nature, and can be excited by light of suitable frequency. If continuous surfaces are present, the extended SP's can then be excited as well. The excitations of either PP or SP result in creating a strong local field close to the metal surfaces. This induced electromagnetic field then polarizes the Raman molecules adsorbed on the metal surfaces, and gives rise to electric dipoles that are oscillating at Raman frequencies. In addition to this direct radiation of Raman signals, the vibrating molecules in turn polarize the metal particles and reenhance their electric dipole moments. It is this multienhancing process that generates a huge enhancement to Raman signals with metal particles and roughened metal surfaces act as an antenna in amplifying Raman signals.[2]

In this paper, we report studies made on the SERS activities of gas-evaporated Ag films. Both the transmission electron microscope (TEM) images and the atomic force microscope (AFM) images of the films show that they consist of Ag nanoparticles (AGN's). And the AGN's in the films fabricated at low evaporation rates are well separated, while those in the films fabricated at high evaporation rates are highly aggregated. The mean grain sizes of the AGN's, on the other hand, show only small deviations from one film to the others. The differences on the optical properties among the films are hence mainly caused by the differences on the degree of aggregation of the AGN's in each film, although the size effect is

0163-1829/95/51(7)/4507(9)/$06.00 ©1995 The American Physical Society

definitely present. Every film studied shows a surface-plasma resonance (SPR) spectrum that peaks at ~3800 Å with a long tail extending to the visible region. These observations indicate that, although it may not be efficient, PP and SP can be created by visible light. And the interplay between SPR and SERS can be studied using visible light as the excitation source. In emphasizing the EM effect, the SERS activities were studied using the Kretschmann's attenuated total reflection (ATR) method,[19] with benzoic acid (C_6H_5COOH) being the reference molecules. The relation between SERS activities and the excitations of PP and SP was studied by means of simultaneously measured SERS spectrum and the intensity of reflected light in the ATR geometry. The AGN films were found to be good enhancers of Raman signals, and a systematic increase in the enhanced Raman intensities with films fabricated at higher evaporation rate was observed. The SERS intensities are linearly proportional to the energy absorbed at the interface. These observations demonstrate the existence of enhancement effect by AGN's and the aggregation among them. We attribute the SERS activities observed to the excitations of localized PP and extended SP.

II. EXPERIMENTAL DETAILS

Ag nanoparticles were fabricated using the gas-evaporation method, where high-purity bulk silver (99.999%) was heated by a current source and was evaporated in argon atmosphere from a tungsten basket. With careful selections of chamber pressure and evaporation rate, we were able to fabricate AGN's that have mean grain sizes fall in the nanometer scale. The AGN's fabricated were deposited directly onto the substrates that were placed 15 cm above the heater source. Three different types of substrates were used for different measurement purposes: The bases of prisms were used for ATR measurements, while glass slides and Cu grids were used for extinction and surface-analysis measurement. A series of six AGN films was fabricated with a mass thickness fixed at 100 Å, a chamber pressure fixed at 1.5 torr of Ar atmosphere, and evaporation rates varying from 0.05 to 5 Å/s. The evaporation rates were carefully controlled, and the mass thickness was monitored by a calibrated quartz microbalance.

The surface morphology and the grain-size distribution of the AGN's in each film were analyzed using an AFM as well as a TEM. The AFM images were taken using the Digital Instruments Nanoscope III operated in the Tapping Mode, where a noncontact technique, with the cantilever tip vibrating at a large amplitude to avoid trapping, was used to profile sample surface. The scan speed was three lines per second, and scan ranges covering from 0.5×0.5 μm^2 to 2.0×2.0 μm^2 were employed for obtaining conceivable descriptions of the surface. The TEM images were taken using the JOEL 200CX electron microscope operated at an acceleration voltage of 160 kV. The degree of aggregation of the AGN's was found quite sensitive to the evaporation rate used, while the mean particle size was less sensitive to that over the range of evaporation rate studied.

Colorless benzoic acid was used as the reference molecules, and only a very thin layer of benzoic acid was deposited on top of the AGN films for emphasizing the enhancement effect by AGN's. A drop of the solution of benzoic acid dissolved in ethanol (0.15 mg/ml) was spotted onto an AGN film, followed by spinning the film at 1500 rpm for 30 sec to reduce the accumulation of the benzoic-acid molecules and obtain better homogeneity over the film. This standard process of depositing Raman active molecules was frequently employed, and was believed to provide a very thin layer of benzoic acid onto the surfaces of AGN's films.

The SERS spectra were collected using the Kretschmann's configuration[19] of the ATR method, while optical extinction spectra were measured with the conventional setup. In the ATR configuration, the excitation light was directed to impinge upon a lateral face of the prism and it reaches the base of the prism, where AGN's and benzoic acid were deposited, with an incident angle which is greater than the critical angle so that total reflection occurs inside the prism. Raman signals from benzoic acid were excited by the attenuated wave, enhanced by the AGN's, and collected on the opposite side of the prism. To determine the energy being absorbed at the interface, the intensity of the reflected light that emerged from the other lateral face of the prism was also measured. This intensity gives the amount of energy that was absorbed and being used to excite PP's and SP's in AGN film. The advantage of employing ATR geometry is that the SERS intensities and the excitations of PP's and SP's can simultaneously be measured. For each measurement, the incident beam was carefully set to the angle at which SPR shows a maximum absorption and SERS shows maximum intensities. This is technically a crucial step in this study, since we are comparing the SERS intensities from one film to the others. An Ar^+ laser and a He-Ne laser were used as the excitation sources, and the SERS spectra were recorded using the Spex 1404 double monochromator equipped with a photon-counting system.

III. RESULTS AND DISCUSSIONS

Although relatively few mechanisms have been realized, it is nowadays well known that Ag island films and roughened Ag thin films are capable of enhancing Raman signals. Recent studies[20,21] have shown that films consisting of AGN's are also good enhancer of Raman signals. Our aim in the present studies concentrates on the effects of aggregation of AGN's on the SERS enhancement factor, subject to a fixed total volume of AGN present in the films. A series of six AGN films was fabricated at evaporation rates of 0.05, 0.5, 1.0, 2.0, 3.0, and 5.0 Å/s, with chamber pressure fixed at 1.5 torr of Ar atmosphere and mass-thickness fixed at 100 Å. An argon atmosphere of pressure 1.5 torr can, through collisions, take away most of the kinetic energy of the evaporated Ag atoms before they reach the substrate, and form AGN film rather than smooth Ag thin film on the substrate. The surface of the substrate was not completely covered by AGN's as the mass thickness was chosen to fix at 100 Å. We note that

50% of the surface of the substrate will be covered by AGN's if they are well separated and have a mean grain size of 200 Å. The aggregation then reduces the surface area of the substrate that was covered by AGN's, since it results in a higher stacking height. Differences on the size as well as on the degree of aggregation of the AGN's deposited can be expected, whenever different evaporation rates were employed. Knowledge on the surface morphology of the films hence plays an important role in understanding various optical properties we are reporting here.

A. TEM and AFM studies

Surface morphology of the films fabricated were studied using TEM and AFM. Figures 1 show four of the TEM bright-field images of the films fabricated at different evaporation rates. These images provide good overviews to the film surfaces. The magnification is 50×10^3 and the images displayed are with 1.5×1.0 μm^2 field of view. The AGN's shown in Fig. 1(d) are dispersed, while those shown in Fig. 1(a) are aggregated. A progressive increase in the degree of aggregation of the AGN's with an increasing evaporation rate is clearly evident. We believe that the aggregation must have been formed before AGN's reach the substrate. Trying to determine the mean particle sizes using the images shown in Fig. 1 will generate large uncertainties, simply because the magnification is not large enough and the structure of the aggregates are hard to resolve.

The overall degree of aggregation is better revealed by the TEM image, while the AFM image provides a better resolution on determining the grain sizes. The advantages of using AFM are its capability of mapping three-dimensional images of the surface and its flexibility of using nonconducting substrates in supporting the surface being studied. A three-dimensional image allows us to determine the size as well as the stacking height of the AGN's deposited. And using a nonconducting substrate allows in more closely simulating the surface being used in SERS studies. We note that spherical structure will show a hemispherical image when it is viewed using an AFM, since it measures the atomic forces between the object and the probe from the top of the object. Figures 2(a) and 3(a) show the AFM images of the AGN's deposited on glass slides at evaporation rate of 5 and 0.5 Å/s, respectively. The fields of view is 1×1 μm^2, and the z-contrast scale, which is shown on the upper right-hand corner of each figure, provides a quantitative indication of the stacking heights of the AGN's. Individual AGN's are clearly seen in both images shown, and they are spherical in nature. These images clearly demonstrate that our films consist of AGN's rather than Ag islands or flat Ag layers. And the AGN's in the film fabricated at a high evaporation rate are more aggregated than those in the film fabricated at a low evaporation rate. This result is consistent with what the TEM images have indicated. We note that some portions of the images shown in Figs. 2(a) and 3(a) have their heights range up to 100 nm; this is mainly due to the stacking of AGN's. The sudden change in the stacking height frequently causes a technical difficulty in obtaining good quality AFM images due to the trapping of AGN's on the cantilever tip.

It is clear that the images shown in Figs. 2(a) and 3(a) are in good quality for grain-size analysis, and their size distributions are shown in Figs. 2(b) and 3(b), respectively. The size distributions for those films fabricated at low evaporation rates can be described by log-normal distribution function, and as expected they peak at different positions for films fabricated at different evaporation rates. However, the size distribution departs from the log-normal function as the evaporation rate was increased. An almost even distribution on the particle size, ranging from 10 to 80 nm, was obtained for the film evaporated at 5 Å/s, as shown in Fig. 2(b). A higher evaporation rate not only provides more Ag vapors in the chamber but also gives a higher kinetic energy to each of the evaporated Ag atoms, that in turn increase the collision probability among them, and results in producing larger AGN's and forming aggregated AGN's.

The mean grain sizes, which are the number-of-grain weighted average particle diameter, that we obtained for

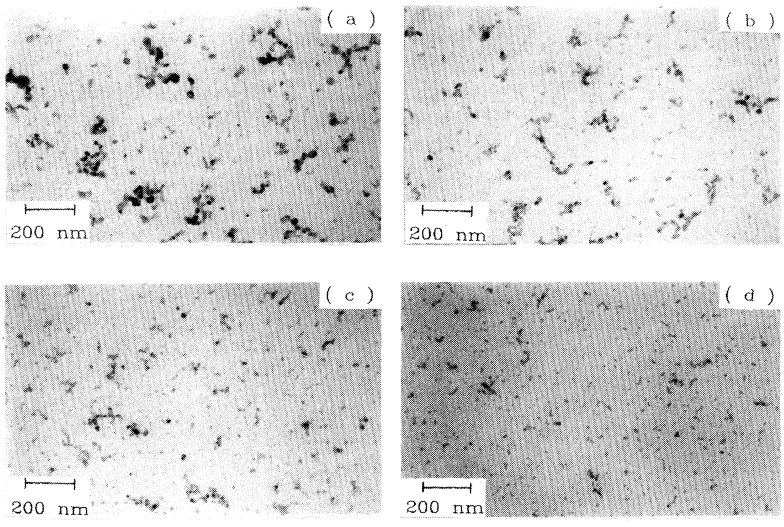

FIG. 1. The TEM bright-field images of the films fabricated at evaporation rates of (a) 5 Å/s, (b) 2 Å/s, (c) 1 Å/s, and (d) 0.5 Å/s. These images provide the overviews of the film surfaces. The AGN's shown in (d) are dispersed, while those shown in (a) are aggregated. A progressive increase in the degree of aggregation of the AGN's with an increasing evaporation rate is clearly evident.

each of the films are listed in Table I. We note that the mean grain size does not, in general, coincide with the peak position. And we choose to quote mean grain size rather than peak position to reflect the size effect, in addition to the aggregation effect, that may contribute to the optical properties discussed below. We did obtain a higher mean grain size for the film fabricated at a higher evaporation rate. Nevertheless, the differences in the mean grain size of the AGN's among each film are less effective than that in the degree of aggregation among AGN's. This is presumably because of a pressure of 1.5 torr, the argon gas in the chamber is not efficient enough in confining Ag atoms to the growth regions. This result suggests that the differences in the SERS activities among each film (see below) are mainly originated from the differences in the degree of aggregation among AGN's rather than in their sizes. Calculations made on summing over (number-of-grain)$\times(\pi/6)\times$(grain-size)^3 for each of the films are listed under the column named total volume in Table I. In the unit of μm^2 Å, the values listed are the mass thickness of the film in unit of Å. They are in good agreement with the values obtained from the thickness monitor. This result supports the argument that the mass thickness of the films is kept fixed. Moreover, it is obvious and clearly shown in Table I that aggregation among AGN's reduces both the total number of grain appearing in the film and the percentage of the surface that was covered by AGN's. About 30% of the substrate surface was covered by AGN's.

TABLE I. Various values obtained from the AFM images of the AGN films fabricated at different evaporation rates.

Evaporation rate (Å/s)	Total number of grain (Counts)	Mean grain size (nm)	Total volume (μm^2 Å)	Coverage (%)
0.05	259	36	115	36
0.5	216	38	115	31
1.0	231	35	100	28
2.0	179	39	105	28
5.0	139	43	110	25

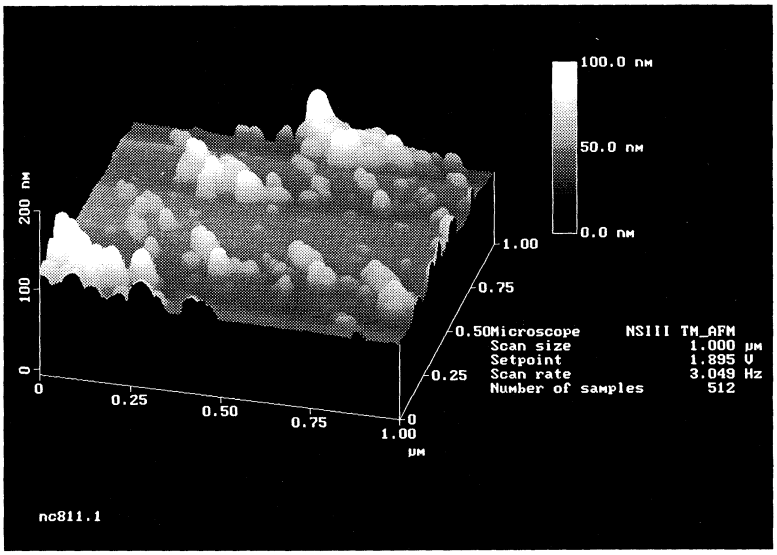

(a)

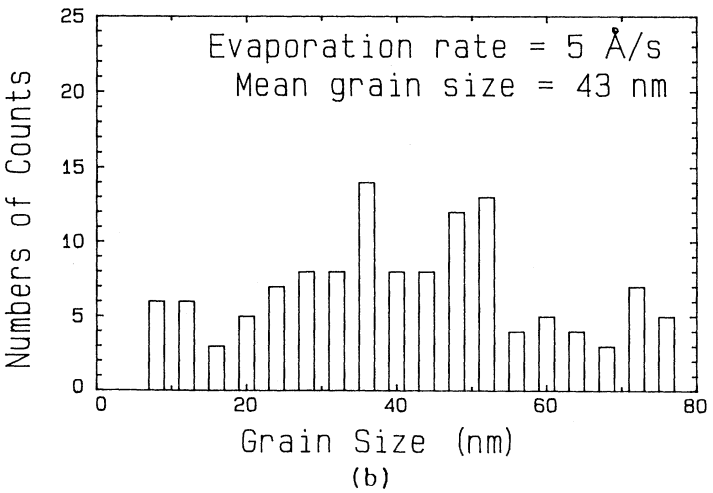

(b)

FIG. 2. (a) The AFM image of the film fabricated at an evaporation rate of 5 Å/s. It clearly shows that the film consists of Ag nanoparticles rather than flat Ag layers, and the AGN's are aggregated. The z contrast, which is shown on the upper right-hand corner, provides a quantitative indication of the stacking heights of AGN's. (b) The size distribution of the AGN's determined from the image shown in (a). An almost even distribution on the particle size is obtained.

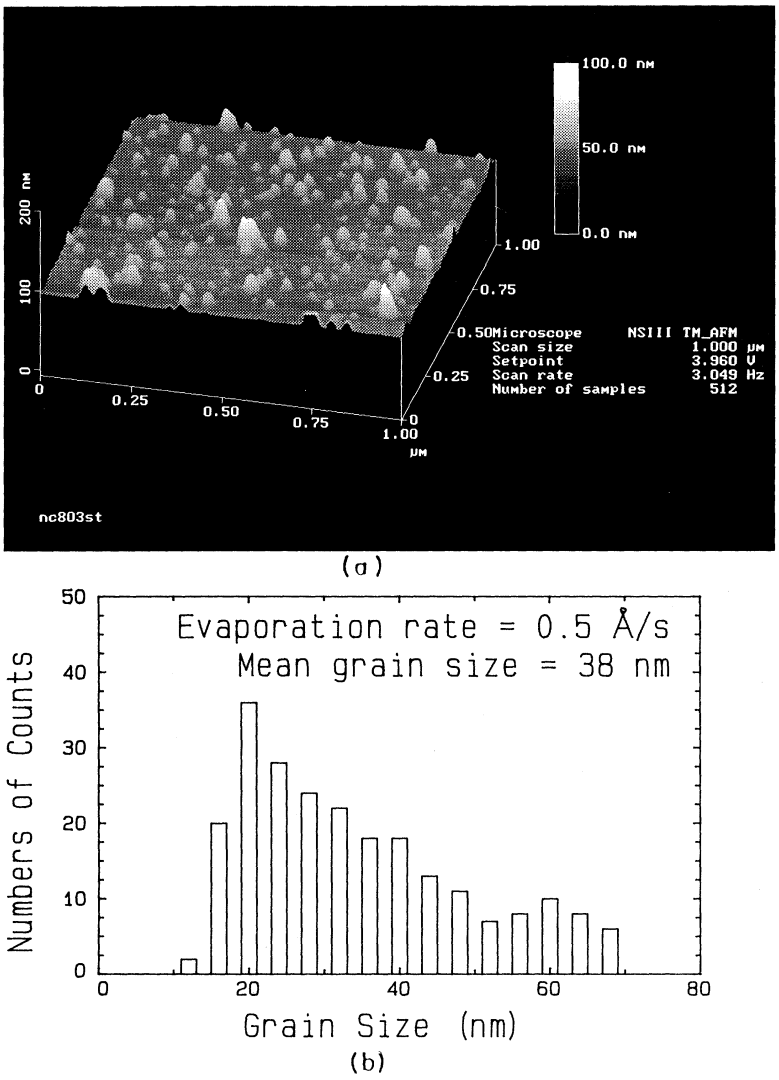

FIG. 3. (a) The AFM image of the film fabricated at an evaporation rate of 0.5 Å/s. Individual AGN's are clearly revealed, and they are dispersed. (b) The size distribution of the AGN's determined from the image shown in (a). The size distribution may be described by a log-normal function.

B. Extinction and surface plasma spectra

Optical transmission spectra were measured using a conventional setup, where a monochromated and collimated light was incident perpendicularly upon the surface of the film, with the detector placed directly on the opposite side of the film to collect the transmitted light. In this setup both the absorbed and the scattered light by AGN's were filtered out, we hence adopt the name extinction instead of absorbance to emphasize this feature. Figure 4 shows the wavelength dependence of the extinction $E \equiv -\log_{10} T$, where T is the transmittance, for four of the AGN films fabricated at different evaporation rates. The spectra were obtained from AGN's being deposited on glass substrates, and the extinction from the glass substrates themselves have been subtracted. We note that the scales used for extinction shown in Fig. 4 are different from one curve to the others, and their multiplication factors are indicated on top of each curve. Figure 4 clearly shows that the extinction for the film deposited at a lower evaporation rate is much smaller than that deposited at a high evaporation rate, and the aggregation among AGN's results in a higher SPR intensity. At peak position, a factor as large as 25 difference on the transmittance were observed between the films deposited at 5 and at 0.25 Å/s. On the other hand, they all show the same extinction profile that exhibits a maximum at ~ 3800 Å with a long tail extending throughout the whole longer wavelength region studied. The maximum, however, does show a small redshift and the width broadens as the evaporation rate was lowered.

We attribute the observed maximal extinction of electromagnetic wave at ~ 3800 Å to the SPR peak of AGN's. The peak position is consistent with a Mie theory[22–24] calculation[20] made for particles that have sizes smaller than 600 Å, and the small redshifts on the peak position for the films fabricated at low evaporation rates are likely due[25] to their smaller mean particle size of the AGN's. The appearance of the long tails on the SPR bands is a direct result of the aggregation among AGN's,[20,26] where additional normal modes arising from interactions between aggregated AGN's need to be accounted for. The existence of the tail in the visible region indicates that PP's and SP's of GNA's can be excited by

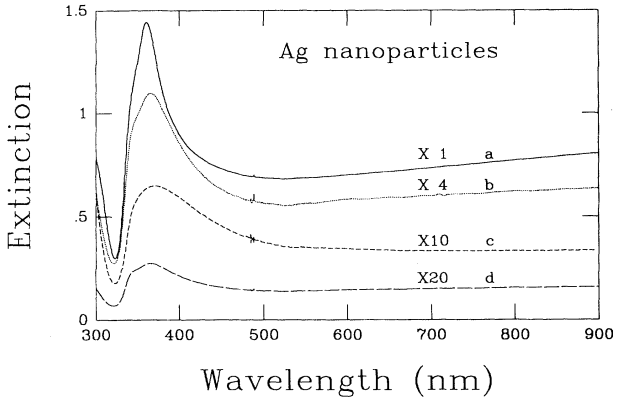

FIG. 4. The optical extinction spectra of AGN's deposited on slide glasses at evaporation rates of (a) 5 Å/s, (b) 2 Å/s, (c) 0.5 Å/s, and (d) 0.05 Å/s. A different scale was used for each curve shown, and the multiplication factor is indicated on top of each curve. The maximal extinction at ~3800 Å is the surface-plasma resonance peak of AGN. The long tail extending to the long-wavelength region observed in each spectrum is a direct result of the aggregation among AGN's.

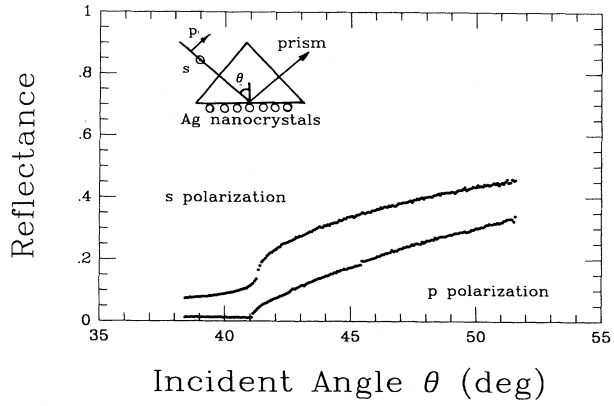

FIG. 5. The reflectance of the excitation light as a function of incident angle measured in the ATR geometry shown in the inset. The absorption of *p*-polarized mode is at every angle greater than that of *s*-polarized mode. It shows that the *p*-polarized mode is more efficient in exciting PP and SP than the *s*-polarized mode does.

visible light, although the SPR spectrum of AGN's peaks at the ultraviolet region. We note that the tails of the extinction curves of the densely-aggregated films are on the increase as extending to the long wavelength region. Its physical origin is not clear to us at this point.

C. SERS activities

The evanescent electromagnetic field that is present in the film region can excite PP and SP of the AGN's, and gives rise to a measurable Raman intensity. In the study of the interplay between the excitations of surface plasma and the enhancement of Raman signals, the ATR geometry was employed where the reflected light and Raman intensity were measured simultaneously with a varying incident angle. By applying ATR geometry, the electromagnetic effect is emphasized over the molecular effect.[29] And the colorless benzoic acid displays no pronounced absorption in the visible region. The surface enhancement effect is therefore dominating the resonance enhancement effect, if visible lights are used for excitation. Based on the above two advantages, we hence employed ATR geometry and used benzoic acid as the reference molecules in study SERS activity of the AGN films. Figure 5 shows the reflectance of the excitation light as a function of incident angle for both the *s*- and *p*-polarized modes measured in the ATR geometry shown in the inset. The spectra were obtained from the film fabricated at an evaporation rate of 0.5 Å/s, and used the 514.5-nm line from an Ar^+ laser as the excitation source. Similar spectral profiles with smaller reflectance were obtained for the films fabricated at higher evaporation rates. As expected, every spectrum shows a turning point near the critical angle θ_c of total reflection, which is of course wavelength dependent. The data shown in Fig. 5 clearly reveal that the resonance absorption of the *p*-polarized mode is at every incident angle greater than that of the *s*-polarized mode, and for both polarizations the absorption becomes weaker as the incident angle was increased. This is in contrast to what was observed in the Ag island films, where a larger resonance absorption at larger incident angles was observed for the *p*-polarized mode.[18]

Applying the ATR method to prism-AGN's-air systems, at incident angles that are greater than θ_c, an evanescent nonpropagating electromagnetic field[27] can penetrate into the AGN region, and excites PP's and SP's within the AGN's.[19] The energy being absorbed at the prism-AGN's interface depends on the strength of the evanescent E field as well as on the energy associated with the dipole oscillations in AGN's. From the symmetry consideration it is clear that the energies associated with a dipole oscillation along all directions in spherical AGN's are the same. The absorptance of spherical AGN's is, therefore, mainly determined by the strength of the evanescent E field. The variation of the E-field intensity at the interface with the incident angle can be easily found, by using Snell's law and the well-known boundary condition that requires the tangential component of the E field be continuous as the boundary is crossed.[28] The amplitude of the penetrated E field decays exponentially with distance from the prism-AGN's interface. And the strength of the E field at the interface for both the *s*- and *p*-polarized modes was found[29] to decrease with increasing incident angle. The decrease in absorption with the increasing incident angle shown in Fig. 5 is then realized as a direct result of a decreasing on the E-field strength. Furthermore, at the interface the E-field intensity of the *p*-polarized mode are at every angle greater than that of the *s*-polarized mode,[29] which then results in greater absorptions for *p* polarization than for *s* polarization as observed. Figure 5 clearly indicates that the *p*-polarized mode is more efficient in exciting PP and SP than the *s*-polarized mode. And the highest

efficiency occurs at the incident angle at which the reflectance shows a minimum. These results suggest that the p-polarized mode should be used and the incident angle should be chosen, in addition to be greater than θ_c, at the reflection minimum for obtaining maximum enhancement and avoid the confusion that may be caused by the refracted light. We note that the excitations are basically done by an uniform time-varying electromagnetic field, since the sizes of the AGN's are considerably smaller than the penetration depth of the evanescent wave.

Figure 6 shows the variation of the intensity of the 1001 cm^{-1} Raman line of benzoic acid versus the absorption of the p-polarized excitation light measured with incident angles lay in the vicinity of θ_c. The spectrum was taken using the film fabricated at an evaporation rate of 5 Å/s, and was excited by the 514.5 nm line from an Ar^+ laser of power 20 mW. Clearly, the Raman intensity increases as the energy absorbed at the interface becomes higher. In ATR geometry, the energy absorbed from the incident light is transferred into a collective motion of surface charges, and both the nonradiative PP (Refs. 30 and 31) and radiative SP (Ref. 32) can be excited simultaneously on the surfaces of aggregated AGN's. The oscillation of the surface charges modifies the nearby electromagnetic field, and results in an enhancement of Raman signals.[9] Figure 6 then displays the relation between the energy being used in exciting surface plasma and the enhanced Raman signals. The solid curve shown is a least-square linearly fit to the data, which indicates that the enhanced Raman signal is in linear proportion to the energy transferred from the incident light over the absorption range studied. Measurements made on other Raman lines of benzoic acid reveal the same behaviors. This linear relationship between SERS intensity and the energy associated with SPR was observed[18] in flat Ag films and in Ag island films as well. However, our data cannot resolve a linear from a quadratic relation between absorption and SERS intensity, simply because the absorption range we have covered was too narrow to tell a difference between these two types of dependence. Our aim, in the present study, was concentrated on the SERS activities, and, therefore, did not pursue further study along this line. Nevertheless, Fig. 6 clearly points out that on comparing the enhancement effect from different films by means of ATR geometry, the incident angle in each of the measurements must be carefully selected so that the SERS shows a maximum in intensity. Furthermore, the excitation wavelength used is far away from the SPR frequency but locates at the tail region of its absorption band, as shown in Fig. 4. The observations of the SERS intensities demonstrate that the enhancement of electromagnetic fields can still be achieved, and the films consisted of AGN's are good enhancers of Raman signals. Much higher enhancements are expected if shorter excitation wavelength that is closer to the SPR peak is used.

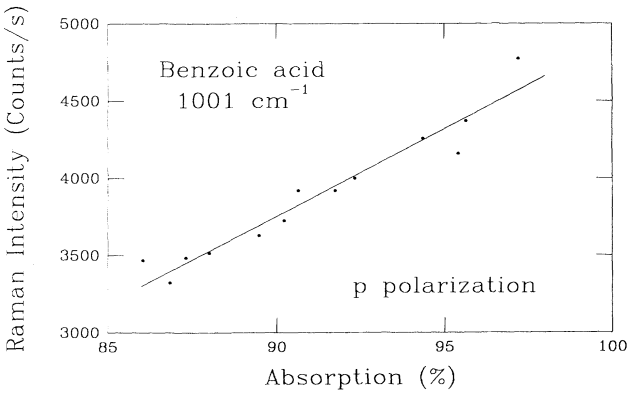

FIG. 6. The relation between the enhanced Raman intensity of the 1001-cm^{-1} line of benzoic acid and the energy being absorbed at the prism-AGN's interface. The spectrum was taken from the film fabricated at 5 Å/s. The solid line is a linear fit to the data, that indicating a linear relationship between SERS intensity and the energy associated with SPR.

Figure 7 shows the enhanced Raman spectra of a thin layer of benzoic acid adsorbed on AGN films fabricated at six different evaporation rates with mass-thickness the fixed at 100 Å. The spectra were obtained using the ATR geometry, and were excited by a 488-nm laser light of power 20 mW. The TEM and AFM images of the films have shown that the aggregation among AGN's progressively increase as a higher evaporation rate was used, while their mean grain sizes fall in the same length scale. The differences on the spectra shown in Fig. 7 are, therefore, mainly caused by the aggregation among AGN's.

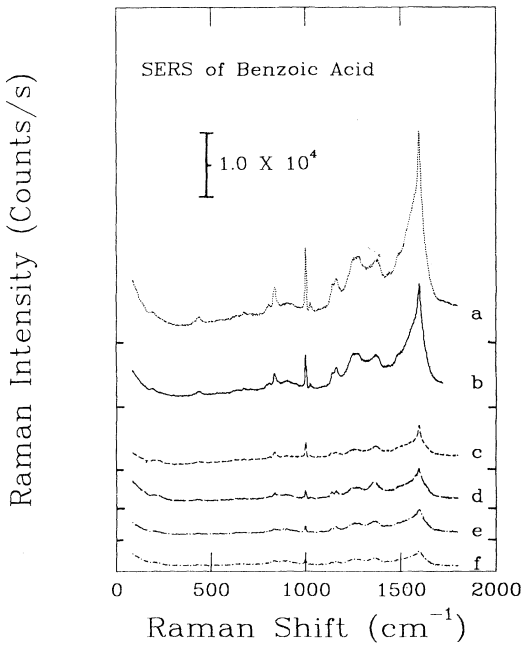

FIG. 7. Enhanced Raman spectra of a thin layer of benzoic acid adsorbed on AGN films fabricated at evaporation rates of (a) 5.0 Å/s, (b) 3.0 Å/s, (c) 2.0 Å/s, (d) 1.0 Å/s, (e) 0.5 Å/s, and (f) 0.05 Å/s. All spectra shown reveal the Raman lines of benzoic acid molecules, and no obvious frequency shift was observed. The enhancements are hence electromagnetic in nature. It clearly shows that the films fabricated at higher evaporation rates give rise to higher enhanced Raman intensities.

The data shown in Fig. 7 clearly reveals a progressive increase in SERS intensity as the evaporation rate was raised, and demonstrates the enhancement effect that was mainly originated from the aggregation among AGN's. Although we observed a monotonical increase in Raman intensity, we believe the enhancement factor will eventually saturate, and then may even be decreasing for densely aggregated films. The SERS spectra taken with films fabricated at even higher evaporation rates did show a decreasing in Raman intensity. We choose not to present those data, because at an evaporation rate exceeding 5 Å/s, technically it becomes difficult for the mass thickness to be well controlled at 100 Å. Moreover, no measurable Raman signals were detected in systems where no AGN's were present. This result, on one hand, reassures the existence of the enhancement effect by AGN's, but on the other precludes the ambition in determining the absolute values of enhancement factor for each film. Nevertheless, the absolute intensities of the fastest-deposited film shown is about an order of magnitude higher than that of the slowest-deposited film shown.

All spectra shown in Fig. 7 reveal the Raman lines of benzoic-acid molecules. No obvious frequency shift with respect to the "normal" Raman lines was observed, which then suggests that the enhancements are mainly electromagnetic in nature. However, three broadbands peaking around 900, 1300, and 1600 cm^{-1} were also evident in all spectra. The broadband peaking around 900 cm^{-1} originates[33] from the Ag_2WO_4 that was present in the surface layer. The tungsten was introduced to the system from the boat that was used to hold the Ag powder for evaporation. On the other hand, the broadband peaking around 1300 and 1600 cm^{-1} are the vibration modes of amorphous carbon.[33–36] The amorphous carbons were introduced to the surface layer because an oil diffusion pump was used during evaporation for maintaining chamber pressure.

The Raman intensities obtained from the most densely aggregated film shown in Fig. 7 is a factor of 7 higher than that obtained from the most loosely aggregated film. The size of the AGN's and the degree of surface roughness are the two dominant physical parameters that may affect the EM mechanism for SERS activities. As we have shown above, the mean particle sizes of the AGN's that we deposited on each of the films are in the same length scale. On the other hand, at a mass thickness at which the AGN's do not cover the whole surface area of the substrate, the aggregation then results in creating more submicroscopic valleys and bumps on the film surface. This is evident from the higher mean surface heights obtained for the films fabricated at higher evaporation rates. It then suggests that the variation on the enhancement effect observed is primarily originated from the differences on the degree of surface roughness among each film. And the fast-deposited forms are better SERS enhancers than the slow-deposited films are. Numerous observations[2,5,8,16,24] have shown that well-separated AGN's can support localized PP's, and the aggregation among them can, in addition, support extended SP's that are propagating within the aggregates. The presence of the isolated AGN's amplifies the immeasurable Raman signals from a very thin layer of benzoic acid into a measurable spectrum as shown in Fig. 7(f). The estimated enhancement factor lies in the order of 10^2. The aggregation among them gives rise to a further amplification to the Raman signals, and results in a spectrum as shown in Fig. 7(a). An additional enhancement factor in the order of 10 was then obtained. The total enhancement factor that we obtained is below the 10^4 expected by the EM model.[2] This is understandable since the frequency of the excitation light used is far away from the SPR frequency, that in turn reduces the efficiency in exciting surface plasma of the AGN's. The field enhancement originated from extended SP's may be smaller than that from localized PP's; our observations shown in Fig. 7 indicates that it is large enough for us to detect.

The enhancement originated from the aggregation among AGN's is even more pronounced, if longer wavelengths were used for excitation. The absolute intensities obtained from the most densely and the most loosely aggregated films studies are different by a factor of 12 and 15 if 514.5 and 632.8 nm laser lights were used, respectively, for excitation. These results are consistent with the extinction spectra shown in Fig. 4, where the densely aggregated films show an upturn while the loosely aggregated films continuously show a decrease in the absorption as a longer wavelength was used. A bigger difference between the enhancement obtained from the densely and the loosely aggregated films may be expected as an even longer wavelength was used for excitation.

IV. CONCLUSIONS

Silver nanoparticles were deposited directly onto various substrates by a gas-evaporation method at different evaporation rates but with the mass thickness fixed at 100 Å. The TEM and AFM images show that the major differences between the films deposited at high and low evaporation rates are the degree of aggregation of AGN's deposited, while their mean particle sizes fall in the same length scale. The differences on the optical properties presented among the films are therefore mainly originated from the aggregation effects, where the dipole-dipole interactions among aggregated AGN's cannot be ignored. A long tail extended to the longest wavelength studied (900 nm) in the extinction spectrum was observed in every film studied, which is believed to arise from the dipole-dipole interactions among the aggregates. The existence of this tail allows us to study the interplay between SERS activities and the excitations of surface plasma using visible excitation lights. Only small redshifts on the peak positions of the SPR spectra for the slow-evaporated films were observed, which are believed to be due to the small decrease in the mean particle sizes. Moreover, the tails of the SPR spectra of the aggregated films show upturns on the long-wavelength side, and the upturn becomes more pronounced as the AGN's are more aggregated. The question on whether there exists a second resonance peak at even longer wavelength for well-aggregated films requires further investigations.

The SERS activities of the AGN's were studied using an ATR method, where the excitations of surface plasma and the SERS activities were measured simultaneously. The enhanced Raman intensities can be described as linearly proportional to the energy transferred to the interface from the incident light, this is the same result as that observed in Ag thin films and in Ag island films. However, a quadratic relation also fit nicely to our data, simply because the range studied on the energy transferred was too narrow to really resolve these two types of relations. Further studies with extended range are needed to draw a definitive conclusion on this point. The enhancement factor depends strongly on the degree of aggregation of the AGN's. With a mass-thickness fixed at 100 Å, the densely-aggregated films give rise to higher enhancements to the Raman signals. And the enhancement obtained from the densely and loosely aggregated films can be different by a factor in the order of 10, and this difference on the enhancement factor may become even bigger if longer wavelengths were used for excitation. On the other hand, a huge increase in the enhancement factor for each of the films can be expected if a shorter wavelength that is closer to the SPR frequency is used for excitation.

The results concluded from the studies made on the angular and polarization dependence of ATR spectra suggest that the enhancement of Raman signals is a direct result of the optical electromagnetic field amplification due to the excitation of surface plasma. The aggregated AGN's support localized as well as extended surface-plasma excitations, and are better Raman enhancers than the dispersed AGN's. In this study, the mass thickness was chosen to be fixed, and the enhancement effect originated from the particle size was ignored. We believe[2,37] that these two physical parameters may also play important roles in the enhancement effect. The dependence of enhancement factor on particle size is currently under investigation.

ACKNOWLEDGMENTS

This research was supported by the National Science Council of the Republic of China under Grant No. NSC82-0208-M008-092, and was partially supported by the Physics Department of the NCU under Grant No. PHYS82-1.

[1]M. Fleischmann, P. J. Hendra, and A. M. McQuillan, Chem. Phys. Lett. **26**, 163 (1974).
[2]A. Wokaun, in *Solid State Physics: Advances in Research and Applications,* edited by H. Ehrenreich and D. Turnbull (Academic, London, 1984), Vol. 28, p. 223.
[3]*Surface Enhanced Raman Scattering,* edited by R. K. Chang and T. E. Furtak (Plenum, New York, 1982).
[4]D. L. Jeanmaire and R. P. van Duyne, J. Electroanal. Chem. **84**, 1 (1977).
[5]G. C. Schatz, in *Fundamentals and Applications of Surface Raman Spectroscopy,* edited by R. L. Garrell, J. E. Pemberton, and T. M. Cotton (VCH, Deerfield Beach, FL, 1993).
[6]A. Otto, I. Mroezek, H. Grabhorn, and W. Akermann, J. Phys. Condens. Matter **4**, 1143 (1992).
[7]R. H. Ritchie, Phys. Rev. **106**, 874 (1957).
[8]W. P. Chen, G. Ritchie, and E. Burstein, Phys. Rev. Lett. **37**, 993 (1976).
[9]M. Moskovits, J. Chem. Phys. **69**, 4159 (1978).
[10]D.-S. Wang and M. Kerker, Phys. Rev. B **24**, 1777 (1981).
[11]B. H. Loo and T. E. Furtak, Chem. Phys. Lett. **71**, 68 (1980).
[12]K. C. Lee and S. S. Chen, Opt. Commun. **67**, 119 (1988).
[13]E. A. Stern and R. A. Ferrell, Phys. Rev. **120**, 130 (1960).
[14]Y. Y. Teng and E. A. Stern, Phys. Rev. Lett. **19**, 511 (1967).
[15]R. Dornhaus, R. E. Benner, R. K. Chang, and I. Chabay, Surf. Sci. **101**, 367 (1980).
[16]S. S. Jha, J. R. Kirtley, and J. C. Tsang, Phys. Rev. B **22**, 3973 (1980).
[17]A. Wokaun, Mol. Phys. **56**, 1 (1985).
[18]Y. T. Wang and K. C. Lee, Surf. Sci. **197**, 239 (1988).
[19]E. Kretschmann, Z. Phys. **227**, 412 (1968).
[20]S. Hayashi, R. Koga, M. Ohtuji, and Yamamoto, Solid State Commun. **76**, 1067 (1990).
[21]C. L. Lei, C. C. Wei, M. C. Chen, S. Y. Ou, W-H. Li, and K. C. Lee (unpublished).
[22]G. Mie, Ann. Phys. (N.Y.) **25**, 377 (1980).
[23]C. F. Bohren and D. R. Huffman, *Absorption and Scattering of Light by Small Particles* (Wiley, New York, 1983).
[24]H. Raether, *Surface Plasmons on Smooth and Rough Surfaces* (Springer-Verlag, New York, 1988).
[25]J. R. Heath, Phys. Rev. B **40**, 9982 (1989).
[26]F. Claro and R. Fuchs, Phys. Rev. B **33**, 7956 (1989).
[27]G. R. Fowles, *Introduction to Modern Optics,* 2nd ed. (Dover, New York, 1989).
[28]J. C. Jackson, *Classical Electrodynamics,* 2nd ed. (Wiley, New York, 1975), Chap. 7.
[29]J. P. Boudonnet, T. Inagaki, E. T. Arakawa, and T. L. Ferrel, Phys. Rev. B **36**, 917 (1987).
[30]A. Otto, Z. Phys. **216**, 398 (1968).
[31]W. H. Weber and G. B. Ford, Phys. Rev. Lett. **44**, 1774 (1980).
[32]R. H. Bjork, A. S. Karakashian, and Y. Y. Teng, Phys. Rev. B **9**, 1394 (1974).
[33]S. Hayashi, R. Koh, K. Yamamoto, and H. Ishida, Jpn. J. Appl. Phys. **28**, 1444 (1989).
[34]J. C. Tsang, J. E. Demuth, P. N. Sanda, and J. R. Kirtely, Chem. Phys. Lett. **76**, 54 (1980).
[35]A. Otto, Phys. Lett. **76**, 54 (1980).
[36]J. P. Goudonnet, G. M. Begun, and E. T. Arakawa, Chem. Phys. Lett. **92**, 197 (1982).
[37]P. Dawson, K. B. Alexander, J. R. Thompson, J. W. Haas III, and T. L. Ferrell, Phys. Rev. B **44**, 6372 (1991).

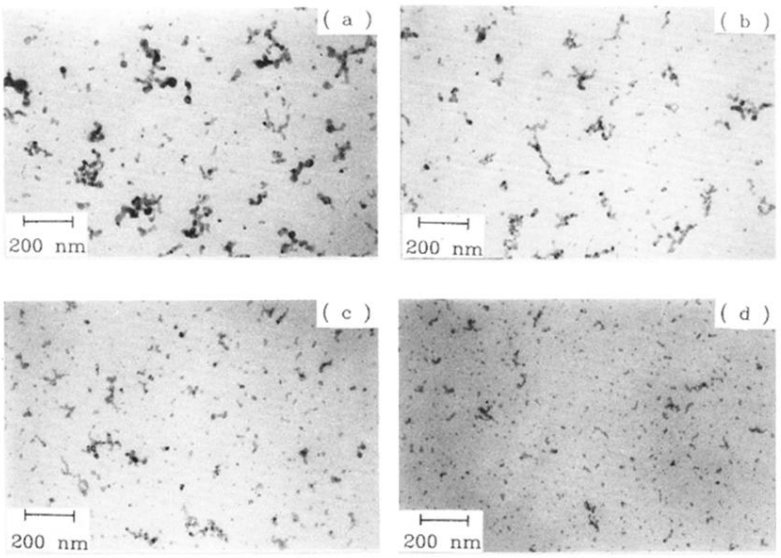

FIG. 1. The TEM bright-field images of the films fabricated at evaporation rates of (a) 5 Å/s, (b) 2 Å/s, (c) 1 Å/s, and (d) 0.5 Å/s. These images provide the overviews of the film surfaces. The AGN's shown in (d) are dispersed, while those shown in (a) are aggregated. A progressive increase in the degree of aggregation of the AGN's with an increasing evaporation rate is clearly evident.

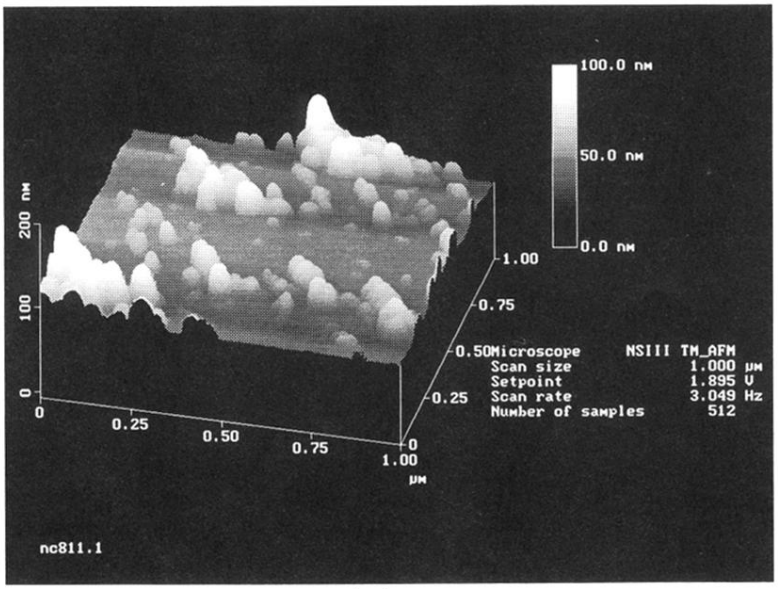

(a)

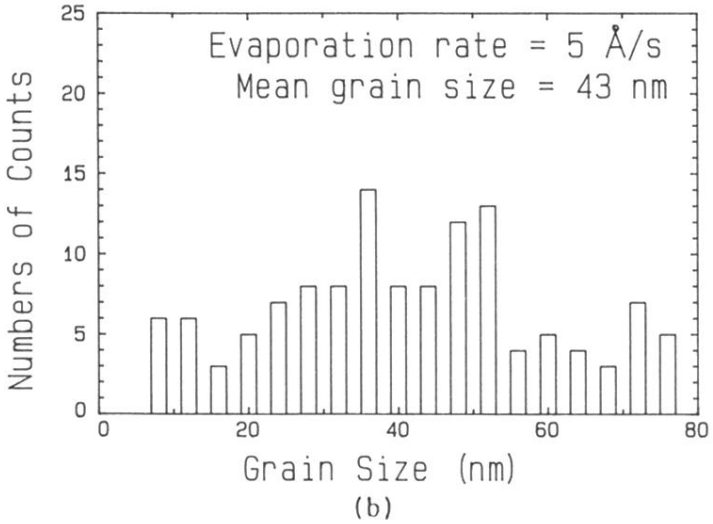

(b)

FIG. 2. (a) The AFM image of the film fabricated at an evaporation rate of 5 Å/s. It clearly shows that the film consists of Ag nanoparticles rather than flat Ag layers, and the AGN's are aggregated. The z contrast, which is shown on the upper right-hand corner, provides a quantitative indication of the stacking heights of AGN's. (b) The size distribution of the AGN's determined from the image shown in (a). An almost even distribution on the particle size is obtained.

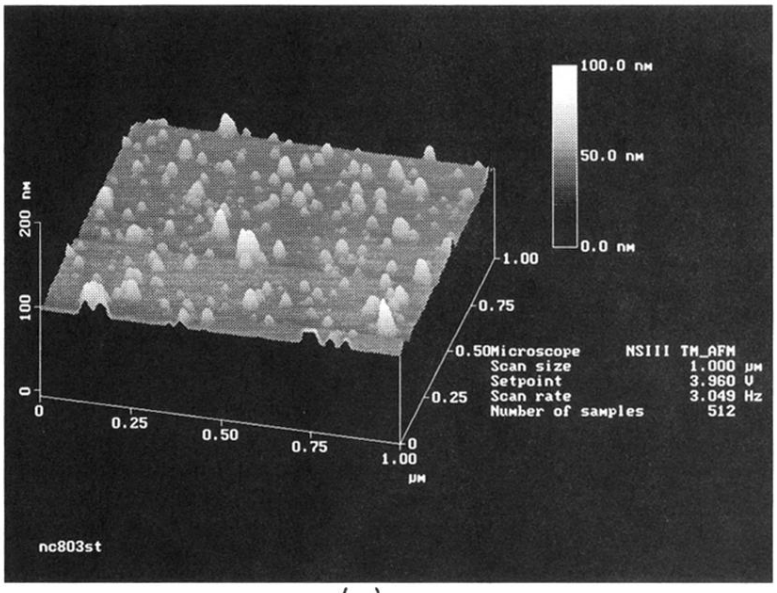

(a)

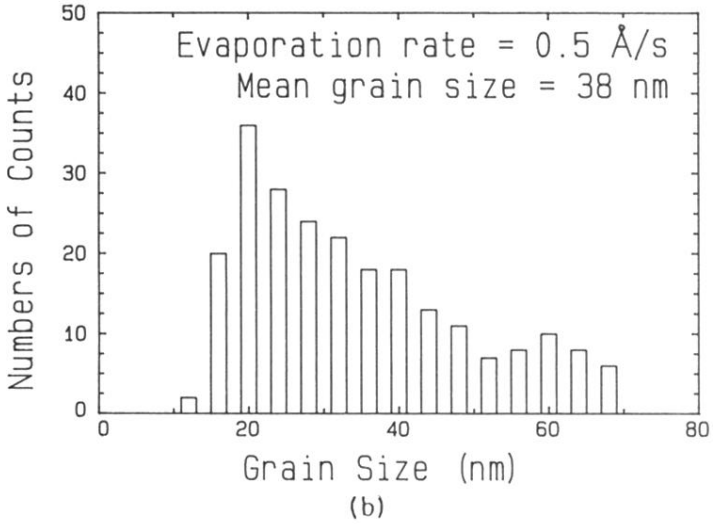

(b)

FIG. 3. (a) The AFM image of the film fabricated at an evaporation rate of 0.5 Å/s. Individual AGN's are clearly revealed, and they are dispersed. (b) The size distribution of the AGN's determined from the image shown in (a). The size distribution may be described by a log-normal function.